Nano Energy 156 (2026) 112174

Contents lists available at ScienceDirect

Nano Energy

journal homepage: www.elsevier.com/locate/nanoen

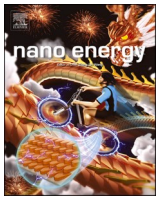

Full Paper

Cellular mechanical phenotyping and therapeutic drug screening in frozen shoulder based on micropillar arrays

Jianfeng Sun [a,b,c], Dengjie Yu [c,d], Changxu Chen [c], Juwei Yang [c,e], Jiaxuan Li [c], Ruizeng Luo [g], Longfei Li [c], Shuo Jin [f,*], Zhuo Liu [g,*], Zhou Li [h,i,j,**], Yusheng Li [a,b,***]

[a] Department of Orthopedics, Xiangya Hospital, Central South University, Changsha 410008, China
[b] National Clinical Research Center for Geriatric Disorders, Xiangya Hospital, Central South University, Changsha 410008, China
[c] Beijing Institute of Nanoenergy and Nanosystems, Chinese Academy of Sciences, Beijing 101400, China
[d] Department of Orthopedics, the Fourth Medical Center of PLA General Hospital, Beijing 100853, China
[e] Department of Cardiology, Fuwai Hospital, National Center for Cardiovascular Diseases, Chinese Academy of Medical Sciences and Peking Union Medical College, Beijing 100037, China
[f] Hepatopancreatobiliary Center, Beijing Tsinghua Changgung Hospital, Key Laboratory of Digital Intelligence Hepatology, Ministry of Education, School of Clinical Medicine, Tsinghua Medicine, Tsinghua University, Beijing 100084, China
[g] Key Laboratory of Biomechanics and Mechanobiology of Ministry of Education, Advanced Innovation Center for Biomedical Engineering, School of Engineering Medicine, Beihang University, Beijing 100191, China
[h] Vita Tech Innovation Center, Tsinghua Changgung Hospital, School of Clinical Medicine, Tsinghua Medicine, Tsinghua University, Beijing 100084, China
[i] School of Biomedical Engineering, Tsinghua University, Beijing 100084, China
[j] Beijing Key Laboratory of Clinical Innovation and Translation for Active Implantable and Interventional Medical Devices, Tsinghua Changgung Hospital, Beijing, 100084, China

ARTICLE INFO

Keywords:
Cellular traction force
Frozen shoulder
Mechanopharmacology
Micropillar arrays

ABSTRACT

Frozen shoulder (FS) is a common musculoskeletal disorder characterized by fibrosis-induced restriction of shoulder movement. Nevertheless, the mechanisms underlying disrupted cellular mechanical homeostasis and the development of effective antifibrotic treatments for FS remain unclear. Cellular traction force (CTF) reflects the mechanical state of cells and is maintained through dynamic interactions between cells and the extracellular matrix. Evaluating CTF is essential for clarifying the mechanisms that contribute to FS fibrosis. In this study, we fabricated force-sensing polydimethylsiloxane micropillar arrays (PDMS-MA) to quantify CTF in synovial cells. Our findings demonstrate that elevated CTF during FS fibrosis is associated with activation of the TGF-β1/SMAD3 pathway, resulting in elevated α-smooth muscle actin (α-SMA) expression and the assembly of focal adhesions (FAs). Using PDMS-MA for mechanopharmacological screening, we identified Pirfenidone and Ketotifen as the most effective compounds at suppressing α-SMA expression, FA assembly, and CTF in fibrotic synovial cells. In vivo experiments further confirmed that Pirfenidone and Ketotifen effectively alleviate shoulder movement restrictions and joint capsule fibrosis. These results suggest that PDMS-MA is a promising tool for mechanopharmacological evaluation and antifibrotic drug screening for FS.

1. Introduction

Frozen shoulder (FS) is a common degenerative inflammatory disorder of the shoulder joint. Epidemiological studies indicate an overall incidence of 2%–5%, which rises significantly to nearly 60% in individuals with systemic conditions such as diabetes[1–3]. FS primarily impacts individuals aged 40–60 years and is 1.6 times more prevalent in women than in men, indicating a significant sex disparity[4,5]. The primary clinical manifestation of FS is persistent shoulder pain accompanied by a significant limitation in both active and passive range

* Corresponding authors.
** Corresponding author at: Vita Tech Innovation Center, Tsinghua Changgung Hospital, School of Clinical Medicine, Tsinghua Medicine, Tsinghua University, Beijing 100084, China.
*** Corresponding author at: Department of Orthopedics, Xiangya Hospital, Central South University, Changsha 410008, China.
E-mail addresses: jsa01263@btch.edu.cn (S. Jin), liuzhuo@buaa.edu.cn (Z. Liu), li_zhou@tsinghua.edu.cn (Z. Li), liyusheng@csu.edu.cn (Y. Li).

https://doi.org/10.1016/j.nanoen.2026.112174
Received 10 May 2026; Received in revised form 20 June 2026; Accepted 30 June 2026
Available online 1 July 2026

of motion (ROM) [6]. This pathology disrupts sleep quality and reduces the capacity for daily activities, thereby negatively impacting patients' physical and psychological health, along with their general social well-being[7,8] . Despite the adverse effects of FS on quality of life, its pathogenesis remains incompletely understood, hindering the development of early diagnostic and effective therapeutic strategies.

Fibrosis is a key pathological process underlying restricted shoulder movement in FS [9]. Similar to fibrotic disorders in other tissues, FS is characterized by abnormal fibroblast recruitment, proliferation, and activation, which promote myofibroblast differentiation, excessive collagen deposition, and progressive thickening and contracture of the joint capsule (Fig. 1**a**) [10]. Under physiological conditions, fibroblasts

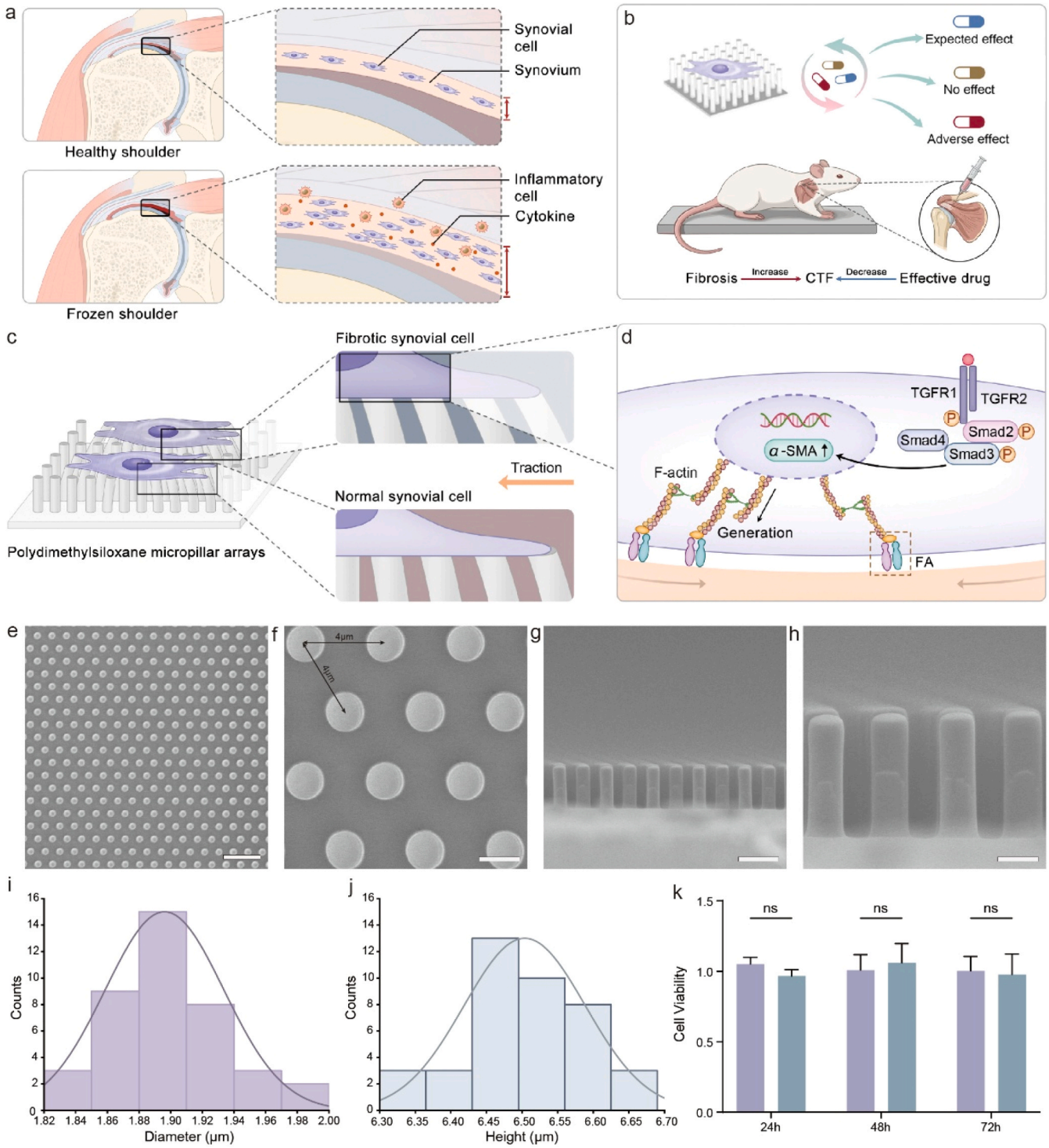

Fig. 1. Schematic overview of the study and characterization of the force-sensing PDMS-MA platform. a) Schematic illustration of the pathogenesis of FS. b) Intended applications of the PDMS-MA. c) The process for synovial cell CTF evaluation. d) Schematic illustration of the mechanism of CTF increase induced by FS. e) Top view of PDMS-MA (scale bar, 10 μm). f) High-magnification top view of PDMS-MA (scale bar, 2 μm). g) Side view of PDMS-MA (scale bar, 4 μm). h) Magnified view of PDMS-MA (scale bar, 2 μm). i) Diameter distribution of the PDMS micropillars ($n = 40$). j) Height distribution of the PDMS micropillars ($n = 40$). k) Comparison of normalized cell viability between leachate and control groups ($n = 3$).

are non-hematopoietic structural cells vital for preserving tissue integrity, supporting development, and promoting injury repair [11]. In the pathological microenvironment of FS, however, persistently elevated concentrations of local cytokines and growth factors compel fibroblasts to synthesize and secrete excessive collagen into the extracellular space. This process leads to substantial deposition of extracellular matrix (ECM) components, increased tissue stiffness, and a subsequent aggravation of joint stiffness and mobility loss [12].

The mechanical properties of tissues reflect a macroscopic expression of cellular mechanical action. Cellular mechanical homeostasis is maintained through dynamic interactions between cells and ECM, with resident cells serving as essential components that provide mechanical support for the tissue [13]. During these interactions, cells generate and transmit mechanical forces to the adjacent ECM through specialized mechanisms; these forces are defined as cellular traction forces (CTF). The generation and transmission of CTF depend on the synchronized activity of the cytoskeleton and focal adhesions (FAs). This enables CTF to influence adjacent cells and the ECM, thereby regulating cellular activities such as proliferation and differentiation, and modifying the physical properties of the tissue microenvironment [14]. Moreover, the composition and structure of the ECM are themselves transcriptionally regulated by these dynamic cell-ECM interactions, thus enhancing the stability of the mechanical microenvironment [15]. Although ECM remodeling is an acknowledged pathogenic characteristic of FS [16], the changes and regulatory mechanisms of cellular mechanical homeostasis during FS progression remain unclear. Conventional fibrosis-related indicators, such as α-SMA expression, collagen deposition, and histological staining, mainly reflect biochemical or structural changes but do not directly quantify the force-generating capacity of fibrotic synovial cells. In contrast, CTF provides a functional readout of actomyosin contraction, focal adhesion-mediated force transmission, and cell–ECM mechanical coupling. Consequently, evaluating CTF dynamics in FS is crucial for understanding cellular mechanical imbalance during fibrosis and for assessing whether candidate drugs can restore mechanical homeostasis in addition to reducing fibrotic marker expression.

We fabricated a regularly structured silicon array mold using high-resolution projection lithography and deep reactive ion etching (DRIE). Using this silicon mold as a template, we subsequently produced the force-sensing polydimethylsiloxane micropillar arrays (PDMS-MA) with a 10:1 ratio of PDMS prepolymer (base to curing agent) (Fig. 1**c**). The PDMS-MA exhibited excellent mechanical stability, facilitating dependable and precise quantification of CTF in synovial cells [17]. We found that abnormal CTF in synovial cells under FS fibrotic conditions is associated with TGF-β1/SMAD3 pathway activation, which upregulates α-smooth muscle actin (α-SMA) and vinculin expression. The increase promotes cytoskeletal remodeling and FA assembly (Fig. 1**d**). Our research provides new insights of the mechanotransduction mechanisms involved in FS pathogenesis, indicating that disrupted cellular mechanical homeostasis contributes to joint fibrosis at the cellular level. Moreover, the PDMS-MA platform shows potential as a tool for mechanopharmacological screening of antifibrotic drugs for FS (Fig. 1**b**).

2. Results

2.1. Fabrication and characterization of PDMS-MA

A key advantage of micropillar arrays for CTF measurement is that each micropillar functions as an independent force sensor. The deflection of each pillar is exclusively caused by the local CTF applied to it, without influence from adjacent pillars [18]. Silicon mold design is a critical step in PDMS-MA fabrication. The diameter and spacing of the micropillars are particularly important, since they influence the sensitivity, spatial resolution, and cell compatibility of the CTF measurements [17]. Specifically, to match the physiological traction force range of synovial fibroblasts, we adjusted the pillar stiffness to achieve a compromise between measurement sensitivity and structural integrity. Considering the standard dimensions of synovial cells and a PDMS elastic modulus of 1.335 MPa, we targeted a pillar height of 6.5 μm (Figure S1, Supporting Information). Although the bulk elastic modulus of PDMS used in this study was higher than the stiffness range of many native soft tissues, the PDMS-MA was designed as a calibrated force-sensing platform rather than a direct mimic of the native soft-tissue mechanical microenvironment. In micropillar-based traction force assays, each pillar functions as an independent elastic cantilever, and the effective force-sensing property is determined not only by the bulk PDMS modulus but also by the pillar geometry, including pillar diameter and height. This arrangement produces a spring constant ideal for detecting force variations in the nano-Newton range while preserving linear elasticity. Consequently, we finalized the micropillar array parameters on the silicon mold as a spacing of 4 μm and a diameter of 2 μm [19–21]. A schematic of the PDMS-MA fabrication and functionalization process is shown in Figure S2. Scanning electron microscopy (SEM) characterization revealed that the micropillar holes on the silicon mold were highly regular (Figure S3a, Supporting Information). Higher-magnification images confirmed a center-to-center distance of 4 μm (Figure S3b, Supporting Information). The hole diameter was measured at 1.90 ± 0.04 μm ($n = 40$), conforming to a normal distribution (Figure S3c, Supporting Information). The resulting PDMS micropillars replicated these dimensions, with a diameter of 1.90 ± 0.04 μm ($n = 40$, Fig. 1**e, f, i**) and a length of 6.50 ± 0.09 μm ($n = 40$, Fig. 1**g, h, j**).

Although PDMS is a commonly used biomedical material with established biosafety and biocompatibility [22], we verified its suitability for long-term culture of synovial cells (RSC−364 cells). PDMS-MA was submerged in cell culture medium for 72 h to prepare a leachate. Synovial cells were then cultured in this leachate for 24, 48, and 72 h. Cell viability was quantitatively assessed using a CCK−8 assay, while live/dead status was examined with Calcein-AM/PI double staining. The results demonstrated that cells treated with PDMS leachates exhibited viability and survival levels comparable to the control group, with no statistically significant differences (Fig. 1**k,** Figure S4, Supporting Information). This confirms that PDMS-MA possesses excellent biocompatibility and is a reliable platform for quantifying CTF in synovial cells.

2.2. Assessment of CTF dynamics during FS fibrosis

Synovial hyperplasia and adhesion formation are core pathogenic features of FS [2]. Transforming growth factor-β1 (TGF-β1), a primary mediator of joint fibrosis [23], is integral to the synovial fibrotic microenvironment of FS [24]. Previous studies have validated the RSC−364 rat synovial cell line as an appropriate *in vitro* model for investigating the pathological mechanisms of shoulder capsule fibrosis and testing therapeutic interventions [25]. To model this pathology, we exposed synovial cells to TGF-β1 to simulate the fibrotic microenvironment and systematically evaluated the CTF response at various time points. CTF was quantified using ImageJ and its related plugins (Fig. 2**a**). Confocal microscopy revealed that synovial cells in both the control and TGF-β1-induced groups caused deflection of the PDMS-MA micropillars. The extent of pillar deflection was significantly greater in the TGF-β1 group compared to the control group, and this difference increased progressively with longer induction times (Fig. 2**b and** Figure S5, Supporting Information). Statistical analysis confirmed a time-dependent increase in CTF following TGF-β1 stimulation. The average CTF in the TGF-β1-treated group was 4.51 ± 0.53 nN at 24 h, slightly higher than that in the control group (3.75 ± 0.43 nN). By 48 h, the mean CTF in the TGF-β1 group increased significantly to 6.28 ± 0.69 nN, whereas the control group remained stable (3.83 ± 0.60 nN), resulting in a more pronounced intergroup difference. At 72 h, CTF in the TGF-β1 group further rose to 6.95 ± 0.91 nN, compared with 3.95 ± 0.65 nN in controls (Fig. 2**c, d**).

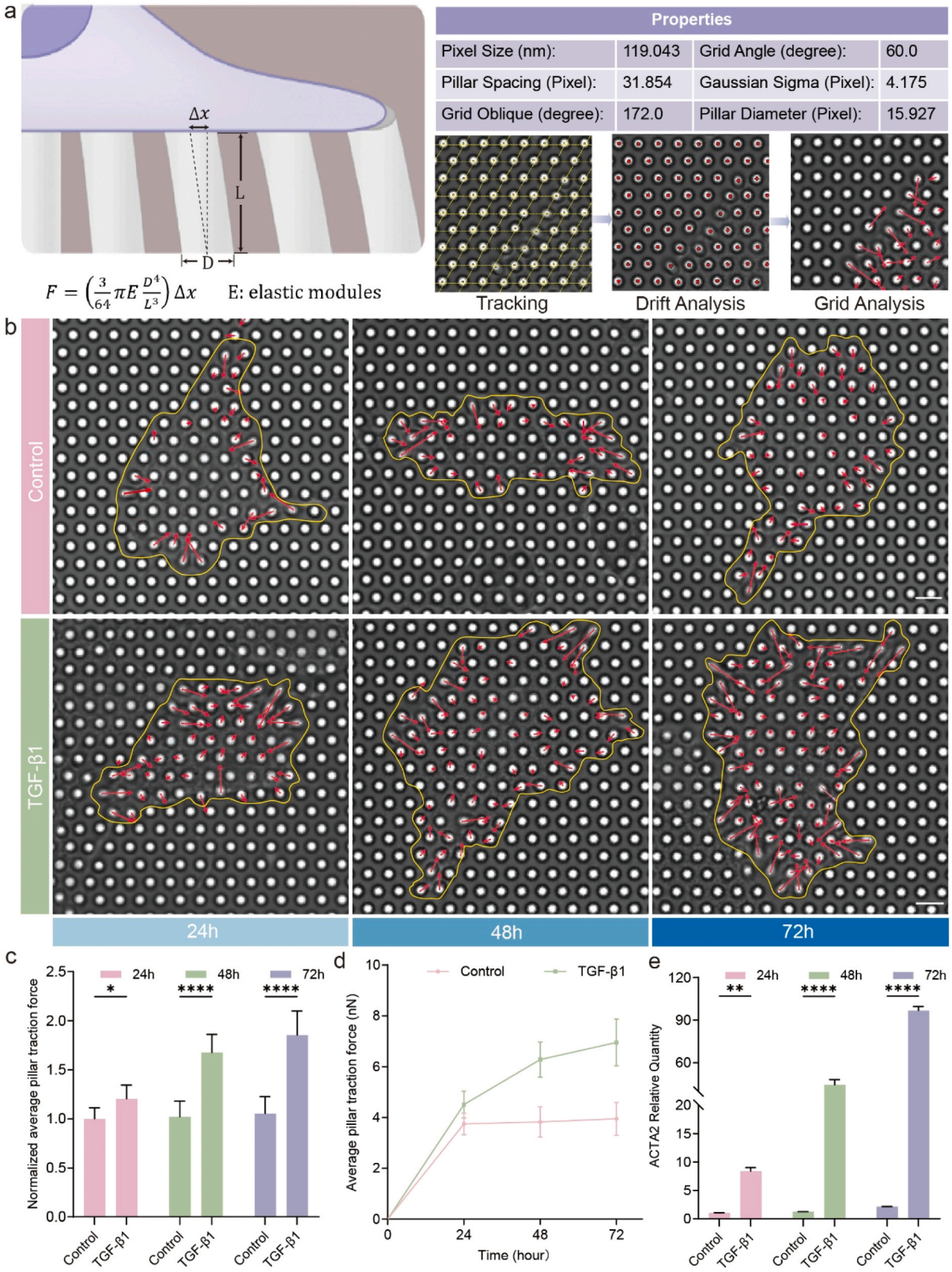

Fig. 2. CTF dynamics and *ACTA2* expression during TGF-β1-induced synovial cell fibrosis. a) Measurement process of CTF. b) Confocal images of normal and TGF-β1 induced synovial cells at different time intervals (scale bar, 5 μm). c) Quantitative analysis of the average pillar traction force ($n = 10$). d) Time-dependent analysis of average pillar traction force. e) Relative mRNA expression levels of *ACTA2* determined by qRT-PCR. Data are presented as mean ± SD. Significance levels: $^{*}p < 0.05$, $^{**}p < 0.01$, $^{****}p < 0.0001$. In the equation, E, D, L and Δx represent the elastic modulus of PDMS, micropillar diameter, micropillar height, and the lateral deflection of the micropillar tip, respectively.

ACTA2, encoding α-SMA, is an established marker of fibroblast-to-myofibroblast transition and ECM synthesis [26]. We measured *ACTA2* expression by quantitative real-time PCR (qRT-PCR) and found it was significantly upregulated in TGF-β1-induced synovial cells relative to the control group. This increase was time-dependent, with a significant rise at 24 h, a more pronounced elevation at 48 and 72 h, and a peak at 72 h (Fig. 2**e**). The continuous upregulation of *ACTA2* indicates a progressive transition of synovial cells to an activated myofibroblast phenotype in response to TGF-β1 stimulation, a trend that correlates with the observed increase in CTF.

To further corroborate the TGF-β1-induced fibrotic phenotype at the ECM level, we examined collagen type I expression and matrix remodeling-related markers. qRT-PCR analysis showed that TGF-β1 markedly upregulated *COL1A1*, *FN1*, and *LOX* expression compared with the control group (Figure S6**,** Supporting Information). *COL1A1* encodes the α1 chain of collagen type I, a major fibrillar collagen associated with collagen-rich fibrotic ECM accumulation and tissue mechanical integrity. *FN1* encodes fibronectin, which can serve as a provisional ECM scaffold that facilitates subsequent collagen assembly and deposition. *LOX* encodes lysyl oxidase, an enzyme involved in collagen fiber cross-linking and matrix stiffening. Consistently, immunofluorescence staining further confirmed a significant increase in collagen I deposition after TGF-β1 stimulation (Figure S7**,** Supporting Information). Together with the increased *ACTA2* expression described above, these results indicate that TGF-β1-induced synovial fibrosis is accompanied by both myofibroblast activation and collagen I-rich ECM remodeling. In addition, qRT-PCR analysis showed that TGF-β1 significantly upregulated *MYH9* expression, whereas *MYH10* showed no significant change (Figure S6**,** Supporting Information), suggesting the involvement of non-muscle myosin IIA in TGF-β1-induced actomyosin-associated contractile activation.

2.3. Mechanism regulating CTF changes during FS fibrosis

After confirming the elevation of CTF in synovial cells during FS fibrosis, we sought to explore the underlying mechanism. CTF is generated and dynamically regulated by the cytoskeletal remodeling and the dynamic assembly of focal adhesions (FAs), enabling cells to respond to microenvironmental signals [14]. Vinculin, an essential structural component of FAs, serves as a principal indicator for evaluating FA dynamics [27]. The canonical TGF-β1/SMAD3 pathway is a principal regulator of fibrosis and promotes fibrotic progression by inducing the expression of fibrotic genes, including collagen and α-SMA [28]. However, it remains unclear whether this pathway is responsible for the abnormal increase in CTF observed in FS fibrosis. We utilized immunofluorescence staining and quantitative analysis to investigate the function of SMAD3 in regulating α-SMA, vinculin, and F-actin organization, as well as its association with CTF dynamics (Fig. 3**a**).

Immunofluorescence analysis showed that TGF-β1 treatment significantly increased α-SMA fluorescence intensity in synovial cells and promoted the formation of dense, well-aligned F-actin stress fibers. Conversely, cells treated with the SMAD3 inhibitor SIS3 alone, or in combination with TGF-β1, displayed α-SMA expression that was nearly imperceptible ($n = 15$; Fig. 3**b, d**). There were no significant differences in the total F-actin fluorescence intensity between the groups (Figure S8**,** Supporting Information). The analysis of vinculin staining indicated that TGF-β1 stimulation significantly increased both the number and mean area of FAs. These effects were suppressed by SIS3 treatment, which significantly reduced FA number and area ($n = 15$; Fig. 3**c, e, f**). At the mechanical level, the average pillar traction force was significantly elevated in the TGF-β1 group (6.38 ± 0.77 nN) compared to the control (4.32 ± 0.44 nN), SIS3-alone (5.08 ± 0.32 nN), and SIS3 + TGF-β1 (5.15 ± 0.47 nN) groups (Fig. 3**g**). Moreover, the variations in traction force among treatment conditions correlated strongly with both α-SMA expression levels and the characteristics of FA assembly. Notably, the total fluorescence intensity of F-actin remained unaltered across all groups, despite a robust and time-dependent elevation of CTF in TGF-β1-treated synovial cells.

To further validate the mechanobiological mechanisms observed in the RSC−364 cell line and eliminate potential cell line-specific effects, we isolated primary rat synovial cells and evaluated their fibrotic and mechanical phenotypes under TGF-β1 induction. Consistent with our previous findings, immunofluorescence analysis revealed that α-SMA expression was significantly upregulated in primary synovial cells after TGF-β1 treatment (Figure S9a**, b,** Supporting Information). Furthermore, TGF-β1 stimulation promoted robust assembly of FAs, as evidenced by a marked increase in the number of vinculin-positive FAs and an expanded mean area of FAs (Figure S9a**, c, d,** Supporting Information). Subsequently, we leveraged the PDMS-MA platform to quantify the mechanical dynamics of these primary cells. The results showed a progressive, time-dependent elevation in CTF at 24 h, 48 h, and 72 h post-induction, which was consistent with the mechanical response observed in the cell line (Figure S9e**, f,** Supporting Information). These primary cell data strongly validate our *in vitro* model and confirm that TGF-β1 disrupts the mechanical homeostasis of synovial cells and exacerbates their fibrotic phenotype.

2.4. Application of PDMS-MA in mechanopharmacological drug screening for FS fibrosis

Current treatments for FS primarily involve anti-inflammatory drugs, with very few options directly targeting fibrosis. To address this, we selected a panel of five representative drugs with distinct pharmacological mechanisms and documented antifibrotic potential to validate our PDMS-MA-based screening platform: Dexamethasone, the clinical standard-of-care glucocorticoid for FS [29]; Pirfenidone, an FDA-approved antifibrotic agent for idiopathic pulmonary fibrosis [30]; Ketotifen, a clinically widely used antihistamine and mast cell stabilizer with emerging preclinical evidence of antifibrotic activity in multiple organ fibrosis models [31,32]; Metformin, a first-line anti-diabetic drug with well-characterized antifibrotic effects in articular diseases [33,34]; and Salvianolic acid B, a natural bioactive compound with reported antifibrotic activity in fibrotic disorders [35].

This study systematically assessed the mechanopharmacological effects of five drugs (Pirfenidone, Ketotifen, Dexamethasone, Salvianolic acid B, Metformin) using the PDMS-MA platform to identify potential antifibrotic drugs for FS. Immunofluorescence and quantitative analysis revealed that Pirfenidone, Ketotifen, and Dexamethasone significantly suppressed the TGF-β1-induced fibrotic phenotype in RSC−364 cells. These drugs significantly diminished α-SMA fluorescence intensity (Fig. 4**a, b**) and *ACTA2* gene expression (Fig. 4**f, h**), decreased FA number and area (Fig. 4**c, d**), and lowered CTF (Fig. 4**g, i**) compared to the TGF-β1-only group. In contrast, Salvianolic acid B and Metformin failed to reduce α-SMA fluorescence intensity (Fig. 4**b**). Moreover, neither compound significantly affected FA parameters, *ACTA2* gene expression, or CTF compared to the TGF-β1 group (Fig. 4**c, d, f-i**). There were no significant differences in the immunofluorescence intensity of F-actin among all groups (Fig. 4**e and** Figure S10**,** Supporting Information). Notably, the regulatory effects of all five drugs on α-SMA expression, FA assembly, and CTF were highly correlated. Among the three effective drugs, Dexamethasone also reduced the TGF-β1-induced fibrotic and mechanical phenotypes, but Pirfenidone and Ketotifen showed a more balanced inhibitory profile across multiple indicators, including α-SMA expression, FA number and area, *ACTA2* expression, and CTF reduction. These findings suggest that Pirfenidone and Ketotifen may provide broader mechanophenotypic correction than Dexamethasone in this *in vitro* FS fibrosis model. In summary, the PDMS-MA-based screening platform directly quantifies drug-induced changes in cellular mechanical phenotypes, offering a novel strategy for developing and translating mechano-targeted antifibrotic therapies for FS.

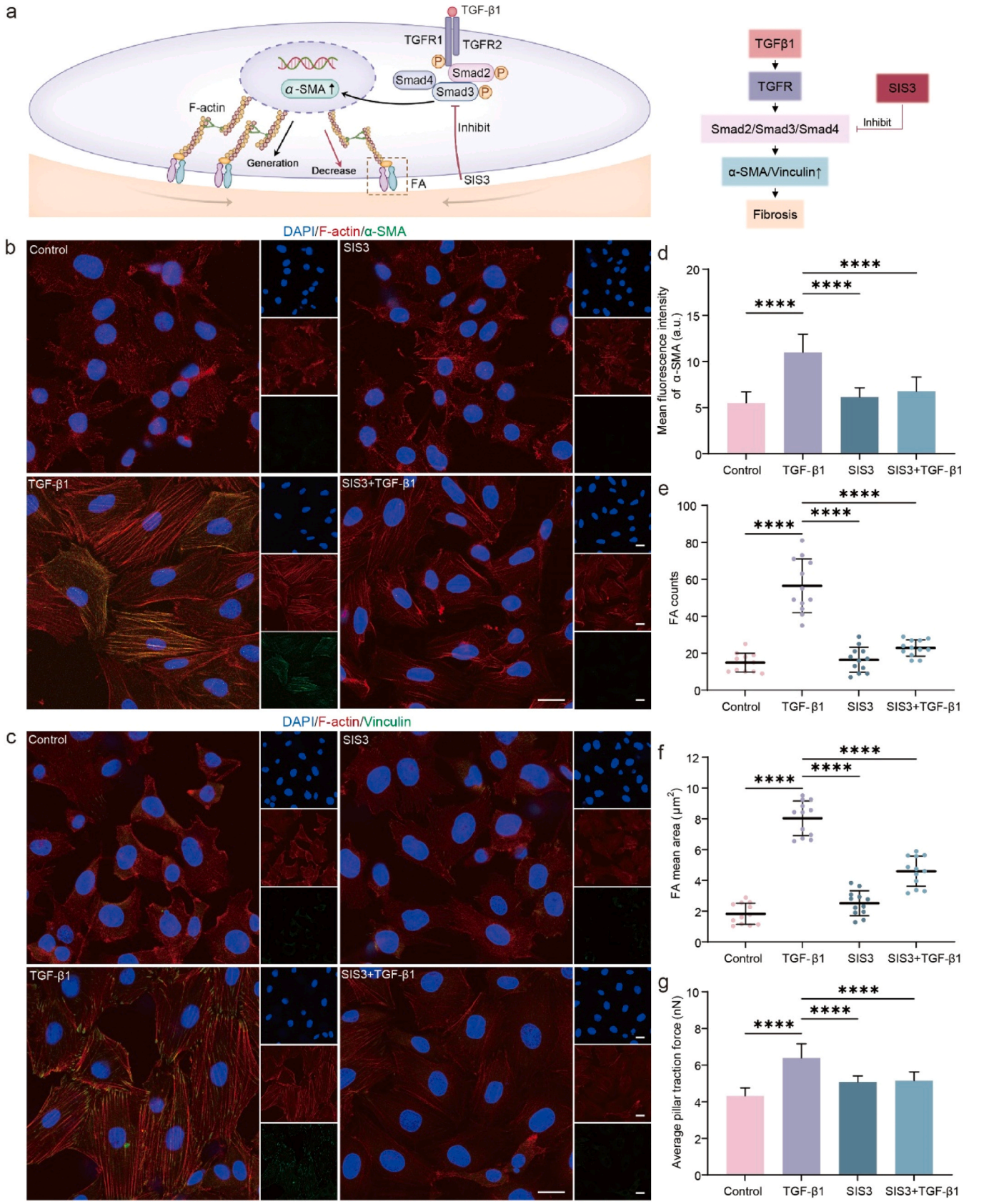

Fig. 3. The TGF-β1/SMAD3 pathway regulates CTF elevation during FS fibrosis by promoting F-actin organization, α-SMA expression, and vinculin assembly. a) Schematic illustration of the TGF-β1/SMAD3 pathway regulating CTF elevation in FS fibrosis. b) Merged confocal images of DAPI, F-actin, and α-SMA in synovial cells. c) Merged confocal images of DAPI, F-actin, and vinculin in synovial cells. d) Mean fluorescence intensity of α-SMA ($n = 12$). e) Quantification of FA counts ($n = 12$). f) Statistical analysis of the mean area of FA ($n = 12$). g) Statistical quantification of the average pillar traction force ($n = 10$). Data are presented as mean ± SD. ****$p < 0.0001$.

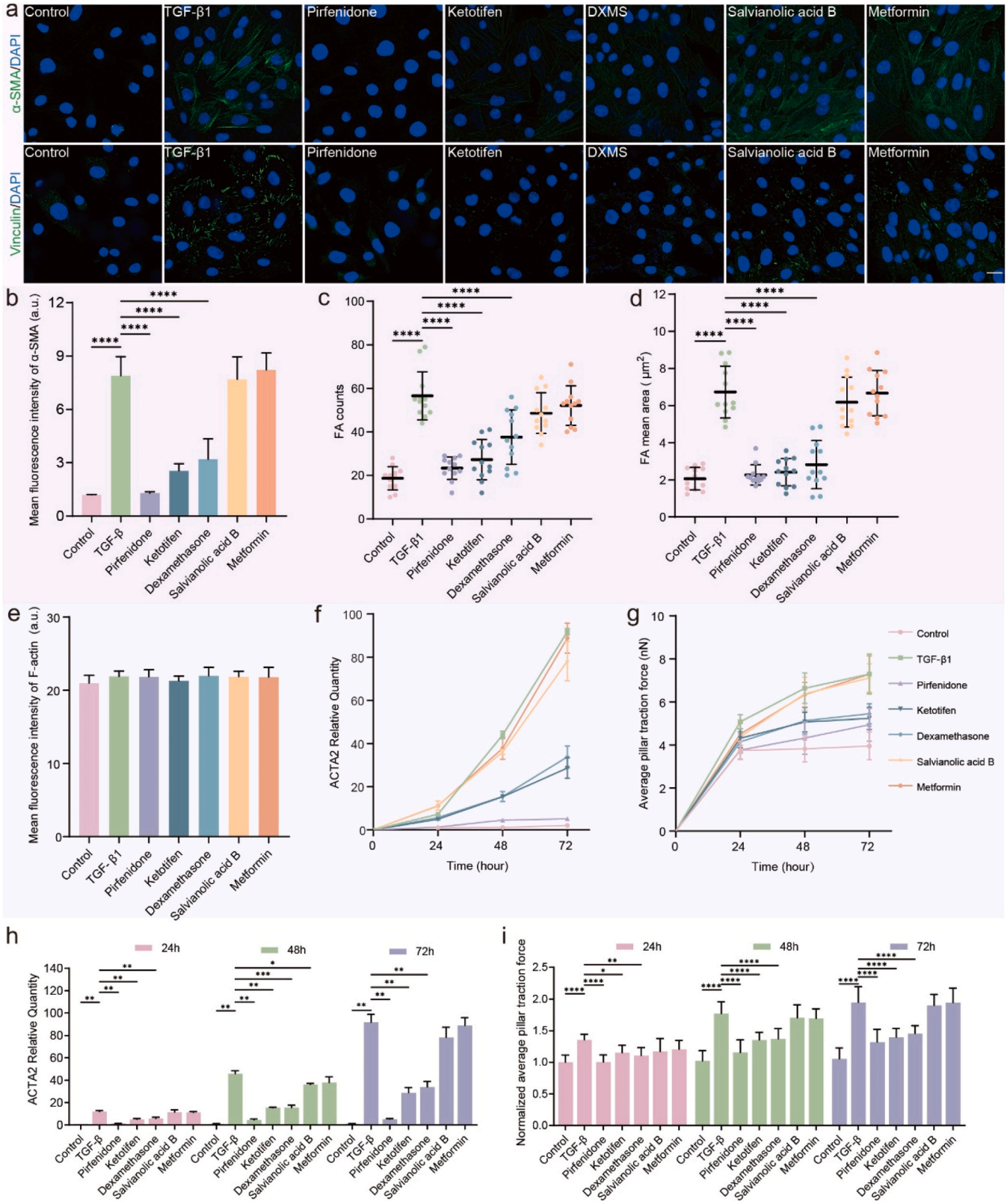

Fig. 4. Drug screening based on CTF in FS fibrotic synovial cells. a) Merged confocal images of DAPI, α-SMA and vinculin in synovial cells (scale bar, 20 μm). b) Quantification of α-SMA mean fluorescence intensity ($n = 12$). c) Quantification of FA counts ($n = 12$). d) Statistical analysis of the mean area of FA ($n = 12$). e) Mean fluorescence intensity of F-actin ($n = 12$). f) Time-dependent analysis of *ACTA2* gene expression ($n = 3$). g) Time-dependent analysis of CTF ($n = 10$). h) *ACTA2* gene expression level assessed by qRT-PCR ($n = 3$). i) Statistical analysis of the average pillar traction force ($n = 10$). Data are presented as mean ± SD. $^{*}p < 0.05$, $^{**}p < 0.01$, $^{***}p < 0.001$, $^{****}p < 0.0001$.

2.5. Biomechanical and antifibrotic efficacy of PDMS-MA-screened drugs in FS rat models

To verify the therapeutic potential of candidate drugs screened via the PDMS-MA platform *in vivo*, we established a rat model of FS using plaster immobilization. Immobilization-based rodent shoulder contracture models have been widely used to reproduce key pathological features of FS [36,37]. Therefore, passive shoulder ROM, capsule thickness, H&E staining, Masson staining, and α-SMA expression were selected as functional, histological, and fibrotic outcome measures, consistent with previous FS and shoulder contracture studies. Compared with the normal control group, the PBS-treated model group exhibited typical FS pathological features, including significantly reduced passive shoulder ROM (Fig. 5**b**) and markedly increased joint capsule thickness (Fig. 5**a, c**). H&E staining revealed synovial hyperplasia and inflammatory cell infiltration, while Masson staining confirmed excessive collagen fiber deposition in the joint capsule. Immunohistochemistry further demonstrated increased α-SMA expression in the joint capsule tissue.

In contrast, interventions with Pirfenidone, Ketotifen, and Dexamethasone all alleviated the above pathological changes. These treatments reduced joint capsule thickening and collagen deposition, attenuated synovial hyperplasia and inflammatory infiltration, and significantly improved passive shoulder ROM in model rats. Dexamethasone was included as a clinically used anti-inflammatory treatment for FS, whereas Ketotifen and Pirfenidone were selected based on their antifibrotic potential identified by our PDMS-MA platform and supported by previous studies in arthrofibrosis and experimental FS models [29,32,38]. Furthermore, quantitative analysis confirmed that these pharmacological treatments significantly reduced the positive area of α-SMA expression compared to the PBS group (Fig. 5**d**). Notably, the *in vivo* reduction of α-SMA expression following drug treatment closely correlated with the decrease in CTF observed in our *in vitro* PDMS-MA screening (Fig. 5**e**).

3. Discussion

Our data indicate that TGF-β1 stimulation is sufficient to induce CTF elevation and fibrotic activation in synovial cells, and that SMAD3 activity is required for this response. Specifically, TGF-β1 increased α-SMA expression, FA assembly, and CTF, whereas SMAD3 inhibition attenuated these effects. Mechanobiologically, the generation and effective transmission of CTF requires two key structural components [13]. The first is the assembly of highly ordered, mechanically competent stress fibers from actin filaments. The well-established myofibroblast contractile marker α-SMA is the primary protein conferring contractility to these stress fibers [39,40]. Our study demonstrated that TGF-β1 stimulation, via SMAD3 activation, significantly upregulated α-SMA expression. This upregulation facilitates the integration of α-SMA into the F-actin cytoskeleton, driving the spatial rearrangement of nascent actin filaments into dense, aligned, and contractile stress fiber bundles, thereby directly augmenting the intrinsic contractile capacity of synovial cells. Interestingly, the total fluorescence intensity of F-actin did not differ significantly among groups, suggesting that CTF elevation was not driven by a global increase in actin polymerization. Instead, the increased α-SMA expression, FA maturation, and CTF indicate that qualitative remodeling of the actin cytoskeleton, including α-SMA incorporation into stress fibers and enhanced cytoskeleton–FA mechanical coupling, is more important for force generation than the total amount of F-actin. The second critical component is the maturation of FAs, which anchor the cytoskeleton to the ECM. Only mature FAs can establish stable mechanical coupling between the cytoskeleton and the ECM, ensuring the effective transmission of intracellular contractile forces to the surrounding matrix [27]. The ECM-related data further extend this mechanobiological interpretation. In the canonical TGF-β signaling pathway, TGF-β receptor activation promotes downstream SMAD2/3 signaling and induces fibrotic gene expression, including α-SMA and collagen type I. Consistent with this mechanism, TGF-β1 stimulation increased both *ACTA2* and *COL1A1* expression in synovial cells. Since collagen type I is one of the main structural components of collagen-rich fibrotic ECM, its increased expression indicates enhanced matrix deposition and provides additional evidence that TGF-β1-induced synovial cell activation involves both myofibroblast differentiation and extracellular matrix remodeling [12,41]. Therefore, TGF-β1-induced FS fibrosis involves a coupled cellular and extracellular mechanical remodeling process: activated synovial cells generate increased CTF through α-SMA, FA, and actomyosin-associated mechanisms, while simultaneously promoting collagen I-rich ECM deposition and matrix stiffness-related remodeling. This functional transmission is quantitatively captured by the elevated CTF detected via our PDMS-MA platform, and our CTF measurements are consistent with those reported in previous studies, supporting the reliability of the experimental data [42,43]. Taken together, these results demonstrate that the TGF-β1/SMAD3 axis drives aberrant CTF elevation in FS fibrosis through functional remodeling of the cytoskeleton and FA system. This process can be effectively reversed by the SMAD3 inhibitor SIS3, further clarifying the core mechanotransduction mechanism of mechanical homeostasis disruption in FS, and laying a theoretical foundation for subsequent mechano-targeted drug screening.

Furthermore, our study highlights the advantages of mechanopharmacology over traditional drug screening. Conventional antifibrotic drug screening primarily depends on tissue-level functional assays or indirect biochemical assessments [44–46]. These methods cannot directly elucidate the dynamic interaction between pharmacological effects and cellular mechanical states, resulting in a disjunction between biochemical processes and mechanical consequences. This may explain why some compounds with promising *in vitro* efficacy exhibit limited therapeutic effects in clinical settings, as they cannot respond appropriately to the *in vivo* mechanical microenvironment or restore cellular mechanical homeostasis [47]. Mechanopharmacology fills this gap by focusing on the bidirectional regulation between cellular mechanics and drug effects [48]. In our study, the *in vivo* reduction of α-SMA expression following drug treatment closely correlated with the decrease in CTF observed in our *in vitro* PDMS-MA screening. This strong correlation bridges macroscopic tissue fibrosis with cellular mechanical states, underscoring the validity of our mechanopharmacological approach. Consequently, integrating mechanopharmacological assessment can enhance the accuracy of drug screening and increase the probability of clinical translation. Nevertheless, CTF should be interpreted as a functional mechanophenotypic indicator rather than as the sole determinant of antifibrotic efficacy. Simply lowering CTF may not be sufficient to reverse established FS fibrosis, because cellular contractility and profibrotic biochemical signaling are mutually reinforcing during fibrosis progression. Therefore, effective FS treatment likely requires both normalization of abnormal cellular mechanics and inhibition of key fibrotic pathways, such as TGF-β1/SMAD3, integrin/FA signaling, Rho/ROCK-mediated actomyosin contractility, and YAP/TAZ mechanotransduction. In our study, Pirfenidone and Ketotifen reduced CTF while also suppressing α-SMA expression, FA assembly, collagen deposition, and joint capsule fibrosis, suggesting that CTF reduction is most meaningful when accompanied by broader inhibition of fibrotic biochemical and structural markers. Among the screened compounds, Ketotifen is particularly attractive from a translational perspective because it is a clinically used antihistamine and mast cell stabilizer with established safety and tolerability in allergic diseases. Recent studies have further shown that Ketotifen can directly attenuate TGF-β1-induced fibrotic responses in human fibroblasts and reduce arthrofibrosis in a rabbit model [31,32]. These features suggest that Ketotifen may have potential value for FS treatment through either local intra-articular administration or systemic administration, although its optimal dosage, intra-articular pharmacokinetics, and long-term safety require further investigation.

There were some limitations in our study. First, although the TGF-β1-

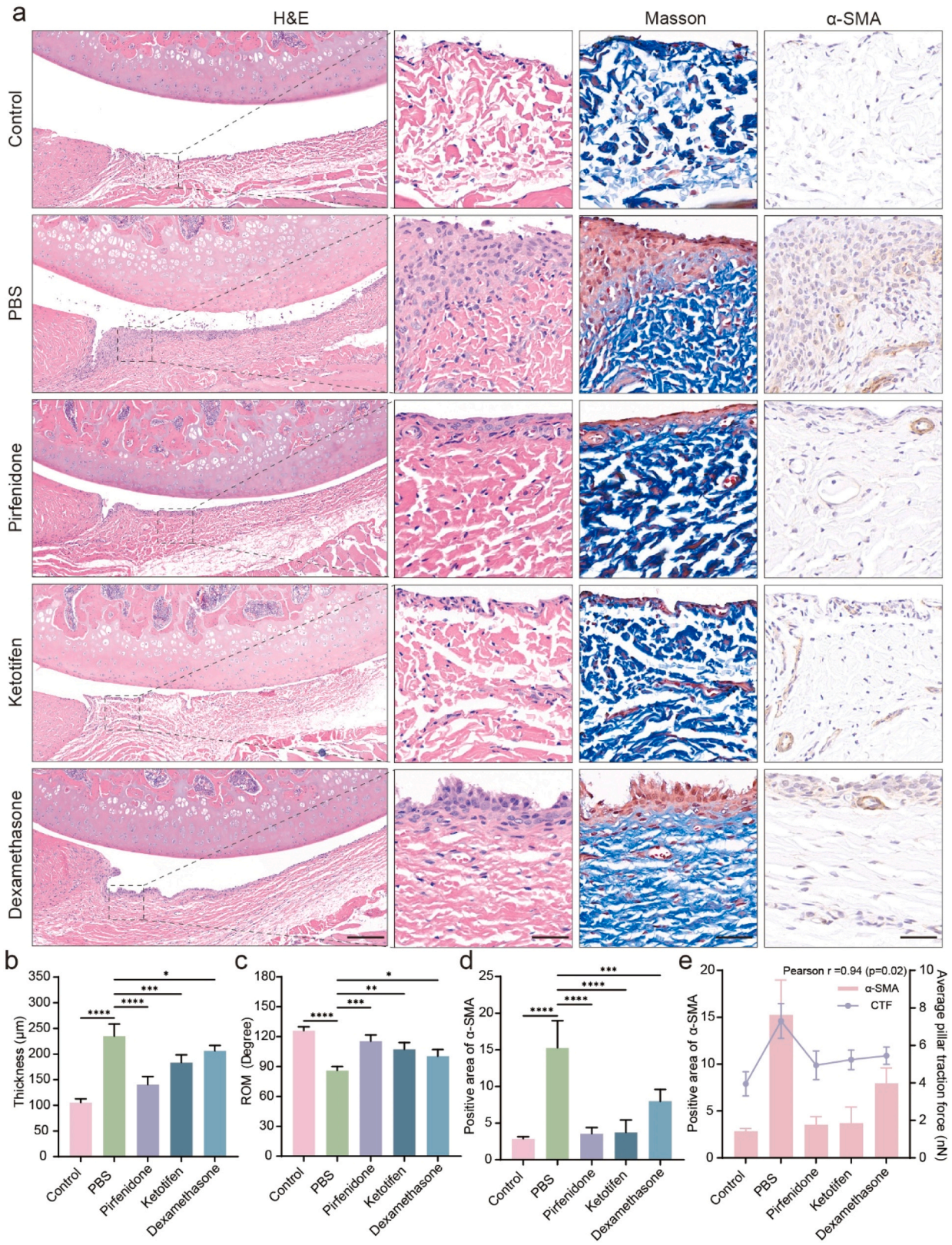

Fig. 5. In vivo antifibrotic efficacy of PDMS-MA-screened drugs in rat FS models. a) H&E staining, Masson's trichrome staining, and α-SMA immunohistochemical staining of the shoulder joint capsule in rats from each group (scale bar: low-magnification field 200 μm, high-magnification field 40 μm). b) Quantitative analysis of the joint capsule thickness in each group ($n = 3$). c) Quantitative statistics of the passive shoulder range of motion (ROM) in rats of each group ($n = 3$). d) Quantitative analysis of the α-SMA positive staining area in the joint capsule tissue from each group ($n = 3$); e) Correlation analysis between in vivo α-SMA expression level and in vitro average CTF in each group. Data are presented as mean ± SD. $^{*}p < 0.05$, $^{**}p < 0.01$, $^{***}p < 0.001$, $^{****}p < 0.0001$.

induced *in vitro* FS fibrosis model was validated in both the rat synovial cell line RSC−364 and primary rat synovial cells, and the therapeutic efficacy was further confirmed in an *in vivo* rat FS model, the phenotypes of these rodent models may still differ from those of primary human FS synovial cells. Therefore, further validation using human clinical samples is warranted. Second, the mechanistic investigation of the TGF-β1/SMAD3-regulated contractile phenotype requires further refinement. Although SIS3 inhibition demonstrated that SMAD3 activity is required for TGF-β1-induced CTF elevation and fibrotic activation, the sufficiency of isolated SMAD3 activation remains to be determined in future studies. In addition, collagen gel contraction assay was not performed in the present study. Since this assay reflects collective matrix-level contraction, future studies combining PDMS-MA-based CTF measurement with collagen gel contraction assays may further clarify the relationship between single-cell traction force and tissue-level collagen matrix contraction during FS fibrosis. Third, the drug screening in this study was limited to five candidate compounds, and formal intra-articular pharmacokinetic and long-term safety evaluations were not included. Expanding future screens to include compounds with diverse structures and mechanisms of action, together with systematic evaluation of local drug retention, clearance, tissue distribution, and safety, will better assess the general applicability and translational potential of the PDMS-MA platform.

4. Conclusion

This study developed a force-sensing PDMS-MA with excellent biocompatibility for the accurate quantification of CTF. We demonstrated that CTF elevation in FS fibrosis is mediated by activation of the TGF-β1/SMAD3 pathway, which promotes α-SMA expression, F-actin organization, and FA assembly. Mechanopharmacological screening using this platform revealed that Pirfenidone and Ketotifen were the most effective among five candidate drugs at reversing the aberrant mechanical phenotypes of FS fibrotic synovial cells. Crucially, the therapeutic potential of these candidates was further validated in an *in vivo* rat model of FS, where they successfully alleviated joint capsule fibrosis and improved shoulder mobility, confirming the predictive value of our *in vitro* platform.

5. Experimental section

5.1. Materials and animals

Recombinant murine TGF-β1 Protein (A279-S390), Pirfenidone (53179–13–8), Ketotifen (34580–13–7), Dexamethasone (50−02−2), Metformin (657−24−9), SIS3 (521984–48–5), and Salvianolic acid B (1221–90–2) were purchased from MedChemExpress LLC (China). Fetal bovine serum (FBS, 10100147) and Collagenase Type II (17101015) were sourced from Gibco (Shanghai, China). Dulbecco's Modified Eagle Medium (DMEM) high glucose (11995), Penicillin-Streptomycin solution (P1400), Trypsin-EDTA solution (T1300), Cell Counting Kit−8 (CCK−8, CA1210), Calcein-AM/PI Double Staining Kit (CA1630), DAPI staining solution (C0060), phosphate buffered saline (PBS, P1020), and normal goat serum (SL038) were obtained from Beijing Solarbio Technology Co., Ltd. (Beijing, China). Antibodies and related reagents, including Anti-Vinculin (ab129002), Alexa Fluor® 488-conjugated Goat Anti-Rabbit IgG H&L (ab150077), and Phalloidin-iFluor 594 Reagent (ab176757), were supplied by Abcam (MA, USA). Alpha Smooth Muscle Actin Polyclonal Antibody (14395–1-AP) was purchased from Proteintech (China). Triton X−100 (ST795), dimethyl sulfoxide (DMSO, ST038), DiI (C1036), and Pluronic F−127 (ST501) were purchased from Beyotime Biotechnology (Shanghai, China). The SYLGARD™ 184 Silicone Elastomer Kit was purchased from Dow Corning (China). Sprague-Dawley rats (female, 7 weeks old) were purchased from Speifu (Beijing) Biotechnology Co., Ltd. All animal experiments were conducted in accordance with the ARRIVE guidelines and the Guide for the Care and Use of Laboratory Animals published by the National Research Council. All experimental procedures were reviewed and approved by the Animal Ethics Committee of the Beijing Institute of Nanoenergy and Nanosystems (2025001LZ).

5.2. Fabrication of PDMS-MA

Silicon array molds were fabricated by high-resolution projection lithography and DRIE [19,49]. The molds were then silanized with trimethylchlorosilane under vacuum for 30 min to facilitate demolding. PDMS prepolymer mixture (base to curing agent ratio of 10:1 by weight) was cast onto the silanized molds, degassed under vacuum, and cured first at 60 °C for 12 h and then at 110 °C for 6 h. Under these curing conditions, the PDMS exhibited an elastic modulus of 1.335 MPa. Finally, the solidified PDMS-MA were carefully peeled off from the silicon molds.

5.3. Cell isolation and culture

The RSC−364 rat synovial cell line was purchased from Shanghai Guandao Bioengineering Co., Ltd. (Shanghai, China). Primary rat synovial cells were isolated from the shoulder joint capsules of Sprague-Dawley rats. Following euthanasia, the synovial tissues of the shoulder joints were carefully harvested under aseptic conditions, washed with PBS, and finely minced. Subsequently, the tissue fragments were digested with a 0.2% type II collagenase solution at 37 °C for 3 h. After digestion, the suspension was filtered through a 70 μm cell strainer and centrifuged to collect the primary cell pellet. For cell culture, DMEM medium was supplemented with 10% FBS and 1% penicillin-streptomycin cocktail, and the cells were incubated at 37 ℃ in a humidified atmosphere containing 5% CO_2.

5.4. Biocompatibility evaluation

The biocompatibility of PDMS-MA was evaluated through a conditioned medium assay followed by Calcein-AM/PI live/dead staining and a CCK−8 assay. To prepare the conditioned medium, PDMS-MA was immersed in cell culture medium for 72 h. RSC−364 cells were seeded into 96-well plates (for CCK−8 assay) and 24-well plates (for fluorescence staining) during the logarithmic growth phase. After 24 h of adhesion under standard culture conditions, the medium was replaced with either PDMS-conditioned medium (experimental group) or fresh medium (control group). After incubation periods of 24, 48, and 72 h, the CCK−8 assay and Calcein-AM/PI staining were performed according to the manufacturer's instructions.

5.5. Induction of FS fibrotic cell model

Unless otherwise stated, RSC−364 cells were used for the main mechanistic and drug-screening experiments, whereas primary rat synovial cells were used only for independent validation experiments. To establish an *in vitro* fibrosis model, synovial cells were cultured in medium supplemented with 10 ng/mL recombinant murine TGF-β1. The SMAD3 inhibitor SIS3 was used at 10 μM to block the TGF-β1/SMAD3 signaling pathway. To evaluate antifibrotic effects, cells were treated with Pirfenidone (250 μM), Ketotifen (25 μM), Dexamethasone (100 nM), Metformin (1 mM), or Salvianolic acid B (50 μg/mL) [25,31,35,50,51].

5.6. Measurement of cellular traction force

The PDMS-MA substrates were functionalized with fibronectin (FN) via microcontact printing to promote cell adhesion [18]. Before seeding cells, the FN-coated substrates were first labeled with 5 μg/mL DiI dye for 1 h at room temperature to enable fluorescence visualization. Subsequently, they were incubated with 0.2% Pluronic F−127 solution for

1 h to prevent nonspecific protein adsorption on the micropillar sidewalls. RSC−364 cells were then seeded in growth medium and allowed to spread overnight. CTF was measured by imaging the samples with a confocal microscope and evaluating PDMS micropillar deflections using PillarTracker 1.1.6 software (Mechanobiology Institute, Singapore). The CTF was calculated based on Euler-Bernoulli beam theory, where pillar deflection was multiplied by the calibrated bending stiffness [42].

5.7. Immunofluorescence staining

RSC−364 cells were seeded on glass-bottomed dishes (35 mm) for immunofluorescence staining. Following fixation with 4% paraformaldehyde and permeabilization using 0.25% Triton X−100 (10 min each at room temperature), nonspecific binding sites were blocked with 10% normal goat serum for 30 min. Samples were then probed overnight at 4 °C using primary antibodies against vinculin (1:250), α-smooth muscle actin (α-SMA, 1:800), and collagen I (1:1000). After washing, an Alexa Fluor 488-conjugated secondary antibody (1:1000) was applied for 1 h in the dark. Cytoskeletal F-actin and cell nuclei were counterstained with Phalloidin-iFluor 594 (30 min) and DAPI (5 min), respectively. Images were captured using a Leica SP8 confocal microscope, and data were analyzed using ImageJ [52].

5.8. Quantitative real-time polymerase chain reaction (qRT-PCR) analysis

Total RNA was isolated from treated cells using TRIzol reagent according to the manufacturer's protocol. RNA concentration and purity were assessed via NanoDrop spectrophotometry. The purified total RNA was reverse-transcribed into complementary DNA (cDNA) using a reverse transcription master mix, and the resulting cDNA was diluted with RNase-free water. qRT-PCR was performed using a SYBR Green master mix on a real-time PCR system. Standard thermocycling conditions consisting of initial denaturation followed by multiple cycles of denaturation and annealing/extension were applied. Amplification specificity was confirmed through melting curve analysis, and relative mRNA expression levels were calculated applying the $2^{-\Delta\Delta Ct}$ method. The primer sequences used in this study are listed in Table S1 (Supporting Information).

5.9. Establishment of animal model

Under anesthesia, the left shoulder joint of each rat was fixed in full adduction and internal rotation, with the elbow joint maintained in flexion and varus position. A plaster bandage was then applied around the left forelimb to immobilize the shoulder joint for 3 consecutive weeks, as previously described in immobilization-based rodent shoulder contracture models [53]. After immobilization, the animals were allowed to resume normal activities. The fixation status of the plaster bandage was examined daily to prevent complications. After 3 weeks of immobilization, the plaster bandage was removed, and the modeled rats were randomly assigned to the PBS, Pirfenidone, Ketotifen, and Dexamethasone groups. Drugs or PBS were administered by a single intra-articular injection into the affected shoulder joint, with the injection volume standardized to 0.1 mL per joint. After injection, the rats were housed under standard conditions for another 1 week. At the end of the study, the rats were euthanized, and passive shoulder ROM was measured according to the method described by Oki et al. [50]. Shoulder joint tissues were then harvested for H&E staining, Masson staining, and immunohistochemical analysis.

5.10. Histological staining

Harvested shoulder tissues were fixed in 4% paraformaldehyde, then subjected to gradient ethanol dehydration and paraffin embedding in sequence, followed by the preparation of serial sections at a thickness of 5 μm. The sections were separately stained with hematoxylin and eosin (H&E), Masson's trichrome, and immunohistochemistry to assess tissue morphological features and target protein expression. The stained sections were observed under a light microscope and images were captured, with subsequent quantitative analysis of relevant indicators conducted using ImageJ.

5.11. Statistical analysis

Data were derived from a minimum of three independent experimental replicates and are expressed as mean ± standard deviation (SD). Statistical analyses were performed utilizing GraphPad Prism software (version 10.1.2). Differences between paired groups were analyzed using two-tailed Student's *t*-tests, while comparisons involving three or more groups utilized one-way ANOVA followed by Tukey's multiple comparison test. All quantitative data were obtained from at least three independent biological replicates. Significance was established at $p < 0.05$, and p-values are indicated as: ns (not significant), * ($p < 0.05$), ** ($p < 0.01$), *** ($p < 0.001$), and **** ($p < 0.0001$).

CRediT authorship contribution statement

Jianfeng Sun: Writing – original draft, Methodology, Investigation, Formal analysis, Data curation, Conceptualization. **Dengjie Yu:** Software, Methodology, Formal analysis, Data curation. **Changxu Chen:** Software, Methodology, Investigation. **Juwei Yang:** Formal analysis, Data curation. **Zhou Li:** Writing – review & editing, Visualization, Validation, Supervision, Project administration, Funding acquisition, Conceptualization. **Yusheng Li:** Writing – review & editing, Visualization, Validation, Supervision, Funding acquisition, Conceptualization. **Shuo Jin:** Methodology, Writing – review & editing, Formal analysis, Supervision. **Jiaxuan Li:** Methodology, Formal analysis. **Ruizeng Luo:** Software, Methodology. **Longfei Li:** Formal analysis, Data curation. **Zhuo Liu:** Writing – review & editing, Visualization, Validation, Supervision, Resources, Project administration, Conceptualization.

Ethics approval and consent to participate

This animal experiment was approved by the Animal Ethics Committee of the Beijing Institute of Nanoenergy and Nanosystems (2025001LZ).

Declaration of Competing Interest

The authors declare that they have no known competing financial interests or personal relationships that could have appeared to influence the work reported in this paper.

Acknowledgements

This work was supported by the National Key R&D Program of China (2024YFC3607600), the National Natural Science Foundation of China (82472522, 92268115, T2125003, U25A20417), the Beijing Natural Science Foundation (L245015, Z240022, 25JL006), the Hunan Provincial Science Fund for Distinguished Young Scholars (2024JJ2089), the Scientific and Technological Innovation Project of China Academy of Chinese Medical Sciences (CI2023C020YL), the Fundamental Research Funds for the General Universities, the Hunan Provincial Innovation Foundation for Postgraduate (CX20250356), and the Independent Exploration and Innovation Project for Postgraduate Students of Central South University (2025ZZTS0178).

Appendix A. Supporting information

Supplementary data associated with this article can be found in the online version at doi:10.1016/j.nanoen.2026.112174.

Data availability

Data will be made available on request.

References

[1] N.L. Millar, A. Meakins, F. Struyf, E. Willmore, A.L. Campbell, P.D. Kirwan, M. Akbar, L. Moore, J.C. Ronquillo, G.A.C. Murrell, S.A. Rodeo, Frozen shoulder, Nat. Rev. Dis. Prim. 8 (2022) 59, https://doi.org/10.1038/s41572-022-00386-2.

[2] N.G. Juel, J.I. Brox, C. Brunborg, K.B. Holte, T.J. Berg, Very High Prevalence of Frozen Shoulder in Patients With Type 1 Diabetes of ≥45 Years' Duration: The Dialong Shoulder Study, Arch. Phys. Med. Rehabil. 98 (2017) 1551–1559, https://doi.org/10.1016/j.apmr.2017.01.020.

[3] D. de la Serna, S. Navarro-Ledesma, F. Alayón, E. López, L. Pruimboom, A Comprehensive View of Frozen Shoulder: A Mystery Syndrome, Front. Med. 8 (2021) 663703, https://doi.org/10.3389/fmed.2021.663703.

[4] K. Kingston, E.J. Curry, J.W. Galvin, X. Li, Shoulder adhesive capsulitis: epidemiology and predictors of surgery, J. Shoulder Elb. Surg. 27 (2018) 1437–1443, https://doi.org/10.1016/j.jse.2018.04.004.

[5] C. Hand, K. Clipsham, J.L. Rees, A.J. Carr, Long-term outcome of frozen shoulder, J. Shoulder Elb. Surg. 17 (2008) 231–236, https://doi.org/10.1016/j.jse.2007.05.009.

[6] A.S. Neviaser, R.J. Neviaser, Adhesive capsulitis of the shoulder, The Journal of, Am. Acad. Orthop. Surg. 19 (2011) 536–542, https://doi.org/10.5435/00124635-201109000-00004.

[7] F. Bagheri, M.H. Ebrahimzadeh, A. Moradi, H.F. Bidgoli, Factors Associated with Pain, Disability and Quality of Life in Patients Suffering from Frozen Shoulder, Arch. Bone Jt. Surg. 4 (2016) 243–247.

[8] E.P. Mulligan, M. Brunette, Z. Shirley, M. Khazzam, Sleep quality and nocturnal pain in patients with shoulder disorders, J. Shoulder Elb. Surg. 24 (2015) 1452–1457, https://doi.org/10.1016/j.jse.2015.02.013.

[9] W.A. Blessing, S.M. Okajima, M.B. Cubria, J.C. Villa-Camacho, M. Perez-Viloria, P. M. Williamson, A.N. Sabogal, S. Suarez, L.H. Ang, S. White, E. Flynn, E. K. Rodriguez, M.W. Grinstaff, A. Nazarian, Intraarticular injection of relaxin-2 alleviates shoulder arthrofibrosis, Proc. Natl. Acad. Sci. USA 116 (2019) 12183–12192, https://doi.org/10.1073/pnas.1900355116.

[10] D.C. Rockey, P.D. Bell, J.A. Hill, Fibrosis–a common pathway to organ injury and failure, New. Engl. J. Med. 372 (2015) 1138–1149, https://doi.org/10.1056/NEJMra1300575.

[11] M.B. Buechler, R.N. Pradhan, A.T. Krishnamurty, C. Cox, A.K. Calviello, A. W. Wang, Y.A. Yang, L. Tam, R. Caothien, M. Roose-Girma, Z. Modrusan, J. R. Arron, R. Bourgon, S. Müller, S.J. Turley, Cross-tissue organization of the fibroblast lineage, Nature 593 (2021) 575–579, https://doi.org/10.1038/s41586-021-03549-5.

[12] N.C. Henderson, F. Rieder, T.A. Wynn, Fibrosis: from mechanisms to medicines, Nature 587 (2020) 555–566, https://doi.org/10.1038/s41586-020-2938-9.

[13] J.D. Humphrey, E.R. Dufresne, M.A. Schwartz, Mechanotransduction and extracellular matrix homeostasis, Nat. Rev. Mol. Cell. Biol. 15 (2014) 802–812, https://doi.org/10.1038/nrm3896.

[14] B.C.H. Cheung, R.J. Abbed, M. Wu, S.E. Leggett, 3D Traction Force Microscopy in Biological Gels: From Single Cells to Multicellular Spheroids, Annu. Rev. Biomed. Eng. 26 (2024) 93–118, https://doi.org/10.1146/annurev-bioeng-103122-031130.

[15] A. Elosegui-Artola, X. Trepat, P. Roca-Cusachs, Control of Mechanotransduction by Molecular Clutch Dynamics, Trends Cell. Biol. 28 (2018) 356–367, https://doi.org/10.1016/j.tcb.2018.01.008.

[16] K.M. Usher, S. Zhu, G. Mavropalias, J.A. Carrino, J. Zhao, J. Xu, Pathological mechanisms and therapeutic outlooks for arthrofibrosis, Bone Res. 7 (2019) 9, https://doi.org/10.1038/s41413-019-0047-x.

[17] M.T. Yang, J. Fu, Y.K. Wang, R.A. Desai, C.S. Chen, Assaying stem cell mechanobiology on microfabricated elastomeric substrates with geometrically modulated rigidity, Nat. Protoc. 6 (2011) 187–213, https://doi.org/10.1038/nprot.2010.189.

[18] D.W. Zhou, M.A. Fernández-Yagüe, E.N. Holland, A.F. García, N.S. Castro, E. B. O'Neill, J. Eyckmans, C.S. Chen, J. Fu, D.D. Schlaepfer, A.J. García, Force-FAK signaling coupling at individual focal adhesions coordinates mechanosensing and microtissue repair, Nat. Commun. 12 (2021) 2359, https://doi.org/10.1038/s41467-021-22602-5.

[19] J. Fu, Y.K. Wang, M.T. Yang, R.A. Desai, X. Yu, Z. Liu, C.S. Chen, Mechanical regulation of cell function with geometrically modulated elastomeric substrates, Nat. Methods 7 (2010) 733–736, https://doi.org/10.1038/nmeth.1487.

[20] M.T. Yang, N.J. Sniadecki, C.S. Chen, Geometric considerations of micro- to nanoscale elastomeric post arrays to study cellular traction forces, Adv. Mater. 19 (2007) 3119, https://doi.org/10.1002/adma.200701956.

[21] S. Inagaki, T. Ishida, Fabrication of Irregularity-Free, Highly Circular Cross-Sectional Microchannel, Micro 2 (2022) 325–333.

[22] I. Miranda, A. Souza, P. Sousa, J. Ribeiro, E.M.S. Castanheira, R. Lima, G. Minas, Properties and Applications of PDMS for Biomedical Engineering: A Review, J. Funct. Biomater. 13 (2021), https://doi.org/10.3390/jfb13010002.

[23] R.S. Watson, E. Gouze, P.P. Levings, M.L. Bush, J.D. Kay, M.S. Jorgensen, E. A. Dacanay, J.W. Reith, T.W. Wright, S.C. Ghivizzani, Gene delivery of TGF-β1 induces arthrofibrosis and chondrometaplasia of synovium in vivo, Lab. Investig. a J. Tech. Methods Pathol. 90 (2010) 1615–1627, https://doi.org/10.1038/labinvest.2010.145.

[24] C. Margadant, A. Sonnenberg, Integrin-TGF-beta crosstalk in fibrosis, cancer and wound healing, EMBO Rep. 11 (2010) 97–105, https://doi.org/10.1038/embor.2009.276.

[25] J. Zhang, Y. Song, L. Zhu, Y. You, J. Hu, X. Xu, C. Wang, J. Lu, Q. Shen, X. Xu, C. Teng, Y. Du, An injectable thermosensitive hyaluronic acid/pluronic F-127 hydrogel for deep penetration and combination therapy of frozen shoulder, Int. J. Biol. Macromol. 263 (2024) 130342, https://doi.org/10.1016/j.ijbiomac.2024.130342.

[26] Y. Zhong, B. Wei, W. Wang, J. Chen, W. Wu, L. Liang, X.R. Huang, C.C. Szeto, X. Yu, D.J. Nikolic-Paterson, H.Y. Lan, Single-Cell RNA-Sequencing Identifies Bone Marrow-Derived Progenitor Cells as a Main Source of Extracellular Matrix-Producing Cells Across Multiple Organ-Based Fibrotic Diseases, Int. J. Biol. Sci. 20 (2024) 5027–5042, https://doi.org/10.7150/ijbs.98839.

[27] C. Grashoff, B.D. Hoffman, M.D. Brenner, R. Zhou, M. Parsons, M.T. Yang, M. A. McLean, S.G. Sligar, C.S. Chen, T. Ha, M.A. Schwartz, Measuring mechanical tension across vinculin reveals regulation of focal adhesion dynamics, Nature 466 (2010) 263–266, https://doi.org/10.1038/nature09198.

[28] X.M. Meng, D.J. Nikolic-Paterson, H.Y. Lan, TGF-β: the master regulator of fibrosis, Nat. Rev. Nephrol. 12 (2016) 325–338, https://doi.org/10.1038/nrneph.2016.48.

[29] Y. Sun, P. Zhang, S. Liu, H. Li, J. Jiang, S. Chen, J. Chen, Intra-articular Steroid Injection for Frozen Shoulder: A Systematic Review and Meta-analysis of Randomized Controlled Trials With Trial Sequential Analysis, Am. J. Sports Med. 45 (2017) 2171–2179, https://doi.org/10.1177/0363546516669944.

[30] T.E. King Jr., W.Z. Bradford, S. Castro-Bernardini, E.A. Fagan, I. Glaspole, M. K. Glassberg, E. Gorina, P.M. Hopkins, D. Kardatzke, L. Lancaster, D.J. Lederer, S. D. Nathan, C.A. Pereira, S.A. Sahn, R. Sussman, J.J. Swigris, P.W. Noble, A phase 3 trial of pirfenidone in patients with idiopathic pulmonary fibrosis, New. Engl. J. Med. 370 (2014) 2083–2092, https://doi.org/10.1056/NEJMoa1402582.

[31] E. Leong, H. Al-Bitar, J.S. Marshall, M. Bezuhly, Ketotifen directly modifies the fibrotic response of human skin fibroblasts, Sci. Rep. 14 (2024) 7076, https://doi.org/10.1038/s41598-024-57776-7.

[32] M.E. Tibbo, A.K. Limberg, C.G. Salib, T.W. Turner, A.R. McLaury, A.G. Jay, J. W. Bettencourt, J.M. Carter, B. Bolon, D.J. Berry, M.E. Morrey, J. Sanchez-Sotelo, A.J. van Wijnen, M.P. Abdel, Anti-fibrotic effects of the antihistamine ketotifen in a rabbit model of arthrofibrosis, Bone Jt. Res. 9 (2020) 302–310, https://doi.org/10.1302/2046-3758.96.Bjr-2019-0272.R2.

[33] Z. Zhu, S. Gao, H. Zhu, Y. Chen, D. Wu, Z. Chen, Y. Huang, X. Wu, N. Hu, D. Chen, W. Huang, H. Chen, Metformin improves fibroblast metabolism and ameliorates arthrofibrosis in rats, J. Orthop. Transl. 40 (2023) 92–103, https://doi.org/10.1016/j.jot.2023.05.011.

[34] S. Rangarajan, N.B. Bone, A.A. Zmijewska, S. Jiang, D.W. Park, K. Bernard, M. L. Locy, S. Ravi, J. Deshane, R.B. Mannon, E. Abraham, V. Darley-Usmar, V. J. Thannickal, J.W. Zmijewski, Metformin reverses established lung fibrosis in a bleomycin model, Nat. Med. 24 (2018) 1121–1127, https://doi.org/10.1038/s41591-018-0087-6.

[35] Q. Liu, J. Lu, J. Lin, Y. Tang, W. Pu, X. Shi, S. Jiang, J. Liu, Y. Ma, Y. Li, J. Xu, L. Jin, J. Wang, W. Wu, Salvianolic acid B attenuates experimental skin fibrosis of systemic sclerosis, Biomed. & Pharmacother. Biomedecine Pharmacother. 110 (2019) 546–553, https://doi.org/10.1016/j.biopha.2018.12.016.

[36] Y. Qiao, J. Wang, L. Zheng, Y. Yang, H. Li, M. Li, S. Zhang, H. Wang, T. Zhang, Proteomics and phosphoproteomics to study Tuina reverses capsule fibrosis in frozen shoulder: a research report based on rats, Sci. Rep. 14 (2024) 661, https://doi.org/10.1038/s41598-023-50904-9.

[37] X. Yuan, S. Feng, W. Xiao, J. Li, Y. He, F. Zhou, X. Liu, Rat shoulder contracture models: Techniques, evaluation, pathophysiology, and applications in developing treatment interventions, Heliyon 10 (2024) e37936, https://doi.org/10.1016/j.heliyon.2024.e37936.

[38] S. Astan, O. Balta, F. Gevrek, Evaluation of the Antifibrotic and Functional Effects of Pirfenidone in an Experimental Frozen Shoulder Model, J. Orthop. Res. Off. Publ. Orthop. Res. Soc. 44 (2026) e70210, https://doi.org/10.1002/jor.70210.

[39] B. Hinz, S.H. Phan, V.J. Thannickal, A. Galli, M.L. Bochaton-Piallat, G. Gabbiani, The myofibroblast: one function, multiple origins, Am. J. Pathol. 170 (2007) 1807–1816, https://doi.org/10.2353/ajpath.2007.070112.

[40] B. Hinz, G. Celetta, J.J. Tomasek, G. Gabbiani, C. Chaponnier, Alpha-smooth muscle actin expression upregulates fibroblast contractile activity, Mol. Biol. Cell. 12 (2001) 2730–2741, https://doi.org/10.1091/mbc.12.9.2730.

[41] H. Devos, J. Zoidakis, M.G. Roubelakis, A. Latosinska, A. Vlahou, Reviewing the Regulators of COL1A1, Int. J. Mol. Sci. 24 (2023), https://doi.org/10.3390/ijms241210004.

[42] A.A. Ketebo, C. Park, J. Kim, M. Jun, S. Park, Probing mechanobiological role of filamin A in migration and invasion of human U87 glioblastoma cells using submicron soft pillars, Nano Converg. 8 (2021) 19, https://doi.org/10.1186/s40580-021-00267-6.

[43] E.N. Holland, D. Lobaccaro, J. Fu, A.J. García, Impact of adhesive area on cellular traction force and spread area, J. Biomed. Mater. Res. Part. A 111 (2023) 609–617, https://doi.org/10.1002/jbm.a.37518.

[44] A. Grosberg, A.P. Nesmith, J.A. Goss, M.D. Brigham, M.L. McCain, K.K. Parker, Muscle on a chip: in vitro contractility assays for smooth and striated muscle, J. Pharmacol. Toxicol. Methods 65 (2012) 126–135, https://doi.org/10.1016/j.vascn.2012.04.001.

[45] C. Wahlquist, D. Jeong, A. Rojas-Muñoz, C. Kho, A. Lee, S. Mitsuyama, A. van Mil, W.J. Park, J.P. Sluijter, P.A. Doevendans, R.J. Hajjar, M. Mercola, Inhibition of miR-25 improves cardiac contractility in the failing heart, Nature 508 (2014) 531–535, https://doi.org/10.1038/nature13073.

[46] J.D. Kijlstra, D. Hu, N. Mittal, E. Kausel, P. van der Meer, A. Garakani, I.J. Domian, Integrated Analysis of Contractile Kinetics, Force Generation, and Electrical

Activity in Single Human Stem Cell-Derived Cardiomyocytes, Stem Cell. Rep. 5 (2015) 1226–1238, https://doi.org/10.1016/j.stemcr.2015.10.017.
[47] K. Galior, V.P. Ma, Y. Liu, H. Su, N. Baker, R.A. Panettieri Jr., C. Wongtrakool, K. Salaita, Molecular Tension Probes to Investigate the Mechanopharmacology of Single Cells: A Step toward Personalized Mechanomedicine, Adv. Healthc. Mater. 7 (2018) e1800069, https://doi.org/10.1002/adhm.201800069.
[48] R. Krishnan, J.A. Park, C.Y. Seow, P.V. Lee, A.G. Stewart, Cellular Biomechanics in Drug Screening and Evaluation: Mechanopharmacology, Trends Pharmacol. Sci. 37 (2016) 87–100, https://doi.org/10.1016/j.tips.2015.10.005.
[49] M. Hashemiesfahan, P. Gelin, H. Gardeniers, W. De Malsche, Enhanced Acoustic Mixing in Silicon-Based Chips with Sharp-Edged Micro-Structures, Micro 4 (2024) 585–598.
[50] M.Y. Yang, Y.J. Lin, M.M. Han, Y.Y. Bi, X.Y. He, L. Xing, J.H. Jeong, T.J. Zhou, H. L. Jiang, Pathological collagen targeting and penetrating liposomes for idiopathic pulmonary fibrosis therapy, J. Control. Release Off. J. Control. Release Soc. 351 (2022) 623–637, https://doi.org/10.1016/j.jconrel.2022.09.054.
[51] H. Xiao, X. Ma, W. Feng, Y. Fu, Z. Lu, M. Xu, Q. Shen, Y. Zhu, Y. Zhang, Metformin attenuates cardiac fibrosis by inhibiting the TGFbeta1-Smad3 signalling pathway, Cardiovasc. Res. 87 (2010) 504–513, https://doi.org/10.1093/cvr/cvq066.
[52] G. Nardone, J. Oliver-De La Cruz, J. Vrbsky, C. Martini, J. Pribyl, P. Skládal, M. Pešl, G. Caluori, S. Pagliari, F. Martino, Z. Maceckova, M. Hajduch, A. Sanz-Garcia, N.M. Pugno, G.B. Stokin, G. Forte, YAP regulates cell mechanics by controlling focal adhesion assembly, Nat. Commun. 8 (2017) 15321, https://doi.org/10.1038/ncomms15321.
[53] D.H. Kim, K.H. Lee, Y.M. Lho, E. Ha, I. Hwang, K.S. Song, C.H. Cho, Characterization of a frozen shoulder model using immobilization in rats, J. Orthop. Surg. Res. 11 (2016) 160, https://doi.org/10.1186/s13018-016-0493-8.